

Singlet-triplet splitting, correlation and entanglement of two electrons in self-assembled InAs/GaAs quantum dot molecules

Lixin He, Gabriel Bester, and Alex Zunger

National Renewable Energy Laboratory, Golden, Colorado 80401

(Dated: February 19, 2019)

Starting with accurate pseudopotential, configuration-interaction treatment of two correlated electrons in vertically coupled self-assembled InAs/GaAs quantum dot-molecules, we show how simpler, popularly-practiced approximations, depict the basic physical characteristics including the singlet-triplet splitting, degree of entanglement (DOE) and correlation. The mean field-like single-configuration approaches such as Hartree-Fock and local spin density, lacking correlation, incorrectly identifies the ground state symmetry and gives inaccurate values for the singlet-triplet splitting and the DOE. The Hubbard model gives qualitatively correct results for the ground state symmetry and singlet-triplet splitting, but produces significant errors in the DOE because it ignores the fact that the strain is asymmetric even if the dots are identical. Finally, the Heisenberg model gives qualitatively correct ground state symmetry and singlet-triplet splitting only for rather large inter-dot separations, but it greatly overestimates the DOE as a consequence of ignoring the electron double occupancy effect.

PACS numbers: 03.67.Mn, 73.22.Gk, 85.35.-p

I. INTRODUCTION

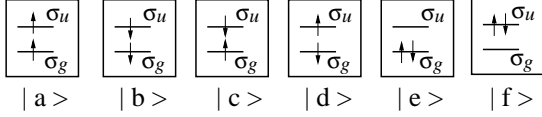
Two vertically^{1,2} or laterally³ coupled quantum dots containing electrons, holes, or an exciton constitute the simplest solid structure proposed for the basic gate operations of quantum computing.^{4,5} The operating principle is as follows: when two dots couple to each other, bonding and anti-bonding “molecular orbitals” (MO) ensue from the single-dot orbitals $\{\chi_i\}$ of the top (T) and bottom (B) dots: $\psi(\sigma_g) = \chi_T(s) + \chi_B(s)$ is the σ -type bonding and $\psi(\sigma_u) = \chi_T(s) - \chi_B(s)$ is the σ -type antibonding state. Similarly, $\psi(\pi_g) = \chi_T(p) + \chi_B(p)$ and $\psi(\pi_u) = \chi_T(p) - \chi_B(p)$ are the “ π ” bonding and antibonding states constructed from the “p” single-dot orbitals of top and bottom dots respectively. Injection of two electrons into such a diatomic “dot-molecule” creates different spin configurations such as $|\sigma_g^\uparrow, \sigma_u^\uparrow\rangle$ or $|\sigma_g^\downarrow, \sigma_u^\downarrow\rangle$, shown in Fig. 1a. In the absence of spin-orbit coupling, these two-electron states are either spin-singlet or spin-triplet states with energy separation J_{S-T} . Loss and DiVincenzo⁵ proposed a simple “swap gate” base on a simplified model where two localized spins have Heisenberg coupling, $H = J_{S-T}(t)\vec{S}_1 \cdot \vec{S}_2$, where \vec{S}_1 and \vec{S}_2 are the spin- $\frac{1}{2}$ operators for the two localized electrons, and the effective Heisenberg exchange splitting $J_{S-T}(t)$ is a function of time t , which is measured as the difference in the energy between the spin-triplet state with the total spin $S = 1$ and the spin-singlet state with $S = 0$. The “state swap time” is $\tau \sim 1/J_{S-T}$. An accurate treatment of the singlet-triplet splitting J_{S-T} and the degree of entanglement carried by the two electrons is of outmost importance for quantum computations.

Theoretical models, however, differ in their assessment of the magnitude and even the sign of the singlet-triplet energy difference J_{S-T} that can be realized in a quantum dot molecule. Most theories have attempted to model dot molecules made of large (50 - 100 nm), electrostatically-

confined^{6,7,8} dots having typical single-particle electronic levels separation of 3 - 5 meV, with larger (or comparable) inter-electronic Coulomb energies $J_{ee} \sim 5$ meV. Such dots are often modeled via a single-band effective-mass approximation (EMA), where multi-band and interval couplings are neglected. Many-body treatments of this simplified EMA model range from phenomenological Hubbard⁹ or Heisenberg^{5,9} models using empirical input parameters, to microscopic Hartree-Fock (HF)^{10,11,12}, local spin densities (LSD) approximation^{13,14} and configuration interaction (CI) method.^{2,15} The LSD-EMA^{13,14} can treat easily up to a few tens of electrons in the quantum dot molecules. However, this approach has shortcoming for treating strongly correlated electrons, predicting for a dot molecule loaded with two electrons that the triplet state is *below* the singlet in the weak coupling region,¹³ as well as incorrectly mixing singlet (spin unpolarized) and triplet (spin polarized) even in the absence of spin-orbit coupling. Since in mean-field approaches like LSD or HF, the two electrons are forced to occupy the same *delocalized* molecular orbitals, the two-electron states are purely unentangled. The Restricted (R)HF method (RHF-EMA) shares similar failures with LSD, giving a triplet as the ground state at large inter-dot separation. The Unrestricted (U) HF corrects some of the problems of RHF by relaxing the requirement of two electrons occupying the same spatial orbital, correctly giving the singlet lower in energy than the triplets.¹² The UHF-EMA can also predict Mott localization of the electrons in the dot-molecule, which breaks the many-particle symmetry.¹¹ However, like the LSD-EMA, the UHF-EMA also incorrectly mixes the singlet and triplet.¹² The CI-EMA has been proven^{2,15} to be accurate for treating few-electron states in large electrostatic dot molecules, and predicts the correct ground state.

The above discussion pertained to large (50 - 100 nm) electrostatic-confined dots. Recently, dot molecules have

(a) Molecular orbital configurations for the dot molecule



(b) Single dot configurations for the dot molecule

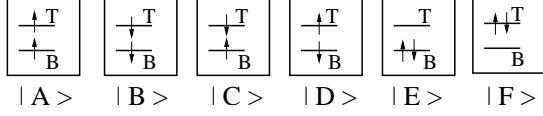


FIG. 1: Possible configurations for two electrons in two vertically coupled quantum dots. (a) Spin configurations in the MO basis. σ_g and σ_u indicate the bonding and anti-bonding states respectively. (b) Spin configurations in the dot-localized basis. “T” and “B” indicate the top and bottom dot.

been fabricated^{16,17} from self-assembled InAs/GaAs, offering a much larger J_{S-T} . Such dot have much smaller confining dimensions (height of only 2 - 5 nm), showing a typical spacing between electron levels of 40 - 60 meV, *smaller* interelectronic Coulomb energies $J_{ee} \sim 20$ meV and exchange energies of $K_{ee} \sim 1$ meV. Such single dots have been accurately modeled¹⁸ via atomistic pseudopotential theories, applied to the single-particle problem (including multi-band and interval coupling as well as non-parabolicity, thus completely avoiding the effective mass approximation). The many-particle problem is then described via all-bound-state configuration-interaction method. Here we use this methodology to study the singlet-triplet splitting in vertically-stacked self-assembled InAs/GaAs dots. We calculate first the singlet-triplet splitting *vs* inter-dot separation, finding the singlet to be below the triplet. We then simplify our model in successive steps, reducing the sophistication with which interelectronic correlation is described and showing how these previously practiced approximations^{10,11,12,13,14} lead to different values of J_{S-T} , including its sign reversal. This methodology provides insight into the electronic processes which control the singlet-triplet splitting in dot-molecules.

The remainder of the paper is arranged as follows. In Sec. II we provide technical details regarding the methodology we use for the calculations. We then compare the singlet-triplet splitting, degree of entanglement and correlation of two-electron states in different levels of approximations in Sec. III. Finally, we summarize in Sec. IV.

II. METHODS

A. Geometry and strain relaxation

We consider a realistic dot-molecule geometry⁴ shown in Fig. 2, which has recently been used in studying ex-

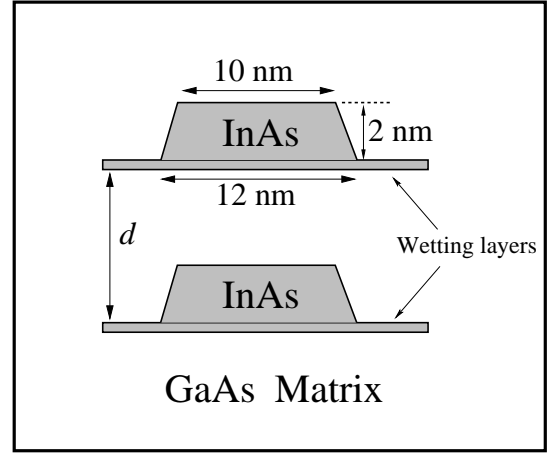


FIG. 2: Geometry of the two vertically coupled quantum dots molecule. The inter-dot distance d is measured from wetting layer to wetting layer.

citon entanglement,^{4,19} and two-electron states.²⁰ Each InAs dot is 12 nm wide and 2 nm tall, with one monolayer InAs “wetting layer”, and compressively strained by a GaAs matrix. Even though experimentally grown dot molecules often have slightly different size and composition concentration for each dot, here we prefer to consider identical dots, so as to investigate the extent of symmetry-breaking due to many-body effects in the extreme case of identical dots. The minimum-strain configuration is achieved at each inter-dot separation d , by relaxing the positions $\{\mathbf{R}_{n,\alpha}\}$ of all (dot + matrix) atoms of type α at site n , so as to minimize the bond-bending and bond-stretching energy using the Valence Force Field (VFF) method.^{21,22} This shows that both dots have large and nearly constant hydrostatic strain inside the dots which decays rapidly outside.²⁰ However, even though the dots comprising the molecule are geometrically identical, the strain on the two dots is different since the molecule lacks inversion symmetry. In fact, we found that the top dot is slightly more strained than the bottom dot. Not surprisingly, the GaAs region *between* the two dots is more severely strained than in other parts of the matrix, as shown in Ref. 20 and as the two dots move apart, the strain between them decreases.

B. Calculating the single-particle states

The single-particle electronic energy levels and wavefunctions are obtained by solving the Schrödinger equations in a pseudopotential scheme,

$$\left[-\frac{\beta}{2} \nabla^2 + V_{ps}(\mathbf{r}) \right] \psi_i(\mathbf{r}) = \epsilon_i \psi_i(\mathbf{r}), \quad (1)$$

where the total electron-ion potential $V_{ps}(\mathbf{r})$ is a superposition of local, screened atomic pseudopotentials $v_\alpha(\mathbf{r})$, i.e. $V_{ps}(\mathbf{r}) = \sum_{n,\alpha} v_\alpha(\mathbf{r} - \mathbf{R}_{n,\alpha})$. The pseudopotentials

used for InAs/GaAs are identical to those used in Ref. 23 and were tested for different systems.^{19,23,24} The factor $\beta=1.23$ is used in Eq.(1) to mimic nonlocal self-energy effects.²³ Equation (1) is solved using the “linear combination of Bloch bands” (LCBB) method,²⁵ where the wavefunctions ψ_i are expanded as,

$$\psi_i(\mathbf{r}) = \sum_{n,\mathbf{k}} \sum_{\lambda} C_{n,\mathbf{k}}^{(\lambda)} \phi_{n,\mathbf{k},\vec{\epsilon}}^{(\lambda)}(\mathbf{r}). \quad (2)$$

In the above equation, $\{\phi_{n,\mathbf{k},\vec{\epsilon}}^{(\lambda)}(\mathbf{r})\}$ are the bulk Bloch orbitals of band index n and wave vector \mathbf{k} of material λ ($=$ InAs, GaAs), strained uniformly to strain $\vec{\epsilon}$. Note that the potential itself still has the inhomogeneous strain dependence. We use $\vec{\epsilon} = 0$ for the (unstrained) GaAs matrix material, and an average $\vec{\epsilon}$ value from VFF for the strained dot material (InAs). For the InAs/GaAs system, we use $n = 2$ (including spin) for electron states on a $6 \times 6 \times 28$ k-mesh. A single dot with the geometry of Fig.2 has 3 bound electron states and more than 10 bound hole states. The lowest exciton transition in the single dot occurs at energy 1.09 eV. For the dot molecule the resulting single-particle states are, in order of increasing energy, the singly degenerated σ_g and σ_u , (bonding and antibonding combination of the s-like single-dot orbitals), and the doubly (nearly) degenerated π_u and π_g , originating from doubly (nearly) degenerate “p” orbitals (split by a few meV) in a single dot. Here, we use the symbols g and u to denote symmetric and anti-symmetric states, even though in our case the single-particle wavefunction are actually asymmetric.²⁰ We define the difference between the respective dot molecule eigenvalues as $\Delta_\sigma = \epsilon(\sigma_u) - \epsilon(\sigma_g)$ and $\Delta_\pi = \epsilon(\pi_g) - \epsilon(\pi_u)$.

C. Calculating the many-particle states

The Hamiltonian of interacting electrons can be written as,

$$H = \sum_{i\sigma} \epsilon_i \psi_{i\sigma}^\dagger \psi_{i\sigma} + \frac{1}{2} \sum_{ijkl} \sum_{\sigma,\sigma'} \Gamma_{kl}^{ij} \psi_{i\sigma}^\dagger \psi_{j\sigma'}^\dagger \psi_{k\sigma'} \psi_{l\sigma}, \quad (3)$$

where, $\psi_i = \sigma_u, \sigma_g, \pi_u, \pi_g$ are the single-particle energy levels of the i -th molecular orbital, while $\sigma, \sigma' = 1, 2$ are spin indices. The Γ_{kl}^{ij} are the Coulomb integrals between molecular orbitals ψ_i, ψ_j, ψ_k and ψ_l ,

$$\Gamma_{kl}^{ij} = \int \int d\mathbf{r} d\mathbf{r}' \frac{\psi_i^*(\mathbf{r}) \psi_j^*(\mathbf{r}') \psi_k(\mathbf{r}') \psi_l(\mathbf{r})}{\epsilon(\mathbf{r} - \mathbf{r}') |\mathbf{r} - \mathbf{r}'|}. \quad (4)$$

The $J_{ij} = \Gamma_{ji}^{ij}$ and $K_{ij} = \Gamma_{ij}^{ij}$ are diagonal Coulomb and exchange integrals respectively. The remaining terms are called off-diagonal or scattering terms. All Coulomb integrals are calculated numerically from atomistic wavefunctions.²⁶ We use a phenomenological, position-dependent dielectric function $\epsilon(\mathbf{r} - \mathbf{r}')$ to screen the electron-electron interaction.²⁶

We solve the many-body problem of Eq.(3) via the CI method, by expanding the N -electron wavefunction in a set of Slater determinants, $|\Phi_{e_1, e_2, \dots, e_N}\rangle = \phi_{e_1}^\dagger \phi_{e_2}^\dagger \dots \phi_{e_N}^\dagger |\Phi_0\rangle$, where $\phi_{e_i}^\dagger$ creates an electron in the state e_i . The ν -th many-particle wavefunction is then the linear combinations of the determinants,

$$|\Psi_\nu\rangle = \sum_{e_1, e_2, \dots, e_N} A_\nu(e_1, e_2, \dots, e_N) |\Phi_{e_1, e_2, \dots, e_N}\rangle. \quad (5)$$

In this paper, we only discuss the two-electron problem, i.e. $N=2$. Our calculations include all possible Slater determinants for the six single-particle basis functions.

D. Calculating pair correlation functions and degree of entanglement

We calculate in addition to the energy spectrum and the singlet-triplet splitting J_{S-T} also the pair correlation functions and the degrees of entanglement (DOE). The pair correlation function $P_\nu(\mathbf{r}, \mathbf{r}')$ for an N -particle system is defined as the probability of finding an electron at \mathbf{r}' , given that the other electron is at \mathbf{r} , i.e.,

$$P_\nu(\mathbf{r}, \mathbf{r}') = \int d\mathbf{r}_3 \dots d\mathbf{r}_N |\Psi_\nu(\mathbf{r}, \mathbf{r}', \mathbf{r}_3, \dots, \mathbf{r}_N)|^2, \quad (6)$$

where, $\Psi_\nu(\mathbf{r}_1, \dots, \mathbf{r}_N)$ is the N -particle wavefunction of state ν . For two electrons, the pair correlation function is just $P_\nu(\mathbf{r}, \mathbf{r}') = |\Psi_\nu(\mathbf{r}, \mathbf{r}')|^2$.

The degree of entanglement is one of the most important quantities for successful quantum gate operations. The DOE of *distinguishable* particles can be calculated from Von Neumann-entropy formulation.^{27,28} For example for a two component system (A, B), the DOE is defined as,^{19,27,28}

$$\mathcal{S} = -\text{Tr } \rho_A \log_2 \rho_A = -\text{Tr } \rho_B \log_2 \rho_B, \quad (7)$$

where, ρ_A and ρ_B are the reduced single-particle density matrices of the subsystems A and B . However, there are some subtleties for defining DOE for *indistinguishable* particles, since it is impossible to separate the subsystems A and B . Recently, we have demonstrated a generalization of the DOE measurement²⁹ for *identical* particles through Slater decompositions.^{30,31} A general two-electron wavefunction can be expanded in the single particle product basis as

$$|\Psi_\nu\rangle = \sum_{a,b=1}^n \omega_{ab} |\psi_a\rangle \otimes |\psi_b\rangle, \quad (8)$$

where ω is an antisymmetric matrix. One can decompose ω_{ab} into a *block diagonalized* matrix in a bi-orthogonal basis,^{30,31} similar to the Schmidt decomposition for two non-identical particles:

$$\omega' = U \omega U^\dagger = \text{diag}[Z_1, Z_2, \dots, Z_r, Z_0], \quad (9)$$

where each block is,

$$Z_u = \begin{pmatrix} 0 & z_u \\ -z_u & 0 \end{pmatrix}, \quad (10)$$

and $Z_0 = 0$. We adopt the normalization condition $\sum_u z_u^2 = 1$, where z_u is a non-negative real number. Alternatively, we could write $\Psi(e_1, e_2)$ in the second quantization representation,

$$\Psi(e_1, e_2) = \sum_u z_u f_{2u-1}^\dagger f_{2u}^\dagger |0\rangle, \quad (11)$$

where, f_{2u-1}^\dagger and f_{2u}^\dagger are the creation operators of $2u-1$ and $2u$ modes. Following Ref.30, it is easy to prove that z_u^2 is an eigenvalue of $\omega^\dagger \omega$. We propose²⁹ to define the DOE for *indistinguishable* fermions as,

$$\mathcal{S} = - \sum_u z_u^2 \log_2 z_u^2. \quad (12)$$

Obviously, if the two-electron wavefunction can be written in a single Slater determinant, only one $z_u=1$ remains and $\mathcal{S}=0$, and the state is *unentangled*. The maximum entanglement of a two-electron system is $\mathcal{S} = \log_2 N$, where N is the number of available single-particle states. It can be shown²⁹ that Eq. 12 reduces to Eq. 7 when the two-electrons are far from each other.

III. RESULTS

Figure 3 shows the bonding-antibonding splitting $\Delta_\sigma(d)$ between the molecular orbitals *vs* inter-dot separation d measured from one wetting layer to the other, showing also the value $\delta_{sp} = \epsilon_p - \epsilon_s$ of the splitting between the p and s orbital energies of a *single dot* (i.e. $d \rightarrow \infty$). The bonding-antibonding splitting decays approximately exponentially as $\Delta_\sigma = 2.87 \exp(-d/1.15)$ eV between $d \sim 4 - 8$ nm. The result of bonding-antibonding splitting includes two competing effects. On one hand, large tunneling distance d certainly reduces the coupling between the two dots; on the other hand, the strain between the dots is also reduced, leading to a lower tunneling barrier, thus increases coupling. The local maximum of Δ_σ at $d=8.5$ nm is a consequence of the this competition. Recent experiments^{16,17} show the bonding-antibonding splitting of about 4 meV at $d=11.5$ nm for vertically coupled InAs/GaAs quantum dots molecules, of similar magnitude as the value obtained here (~ 1 meV), considering that the measured dot molecule is larger (height/base= 4 nm/40 nm rather than 2 nm/12 nm in our calculations) and possibly asymmetric. We also give in Fig. 3 the interelectronic Coulomb energy J_C of a *single-dot* s orbital. We define *strong coupling* region as $\Delta_\sigma \approx \delta_{sp}$, and *weak coupling* region $\Delta_\sigma \ll \delta_{sp}$. We see in Fig. 3 strong coupling for $d \leq 4$ nm, and weak coupling for $d \geq 5$ nm. In the weak coupling region, the π levels are well above the σ levels. We also define

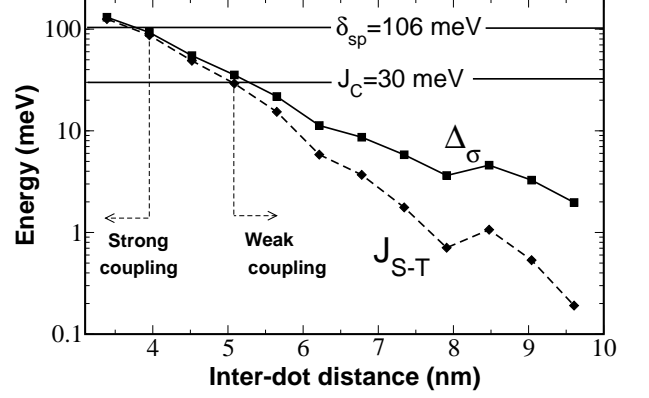


FIG. 3: The bonding-antibonding splitting $\Delta_\sigma = \epsilon(\sigma_g) - \epsilon(\sigma_u)$ (solid line) and singlet-triplet splitting $J_{S-T} = E(^3\Sigma) - E(^1\Sigma_g^{(a)})$ (dashed line) *vs* inter-dot distance d . We also show the single-dot s, p orbitals splitting $\delta_{sp} = \epsilon_s - \epsilon_p$ and the s orbital Coulomb interaction J_C . We define “strong coupling” by $\Delta_\sigma \sim \delta_{sp}$ (< 4 nm) and “weak coupling”, $\Delta_\sigma \ll \delta_{sp}$ (> 5 nm).

“strong confinement” as $\delta_{sp} > J_C$, and weak confinement as the reverse inequality. Figure 3 shows that our dot is in the strong-confinement regime. In contrast, electrostatic dot^{6,7,8} are in the weak confinement regime.

We next discuss the two-electron states in the QDMs and examine several different approximations which we call Levels 1 - 4, by comparing the properties of the ground states, the singlet-triplet energy separation J_{S-T} and the pair correlation functions as well as the degree of entanglement for each state. Starting from our most complete model (Level 1) and simplifying it in successive steps, we reduce the sophistication with which interelectronic correlation is described and show how these previously practiced approximations lead to different values of J_{S-T} (including its sign reversal), and different degree of entanglement. This methodology provides insight into the electronic features which control singlet-triplet splitting and electron-electron entanglement in dot molecules.

A. Level-1 theory: all-bound-state configuration interaction

We first study the two-electron states by solving the CI Eq. (5), using all confined molecular orbitals σ_g, σ_u and π_g, π_u , to construct the Slater determinants. This gives a total of 66 Slater determinants. The continuum states are far above the bound-state, and are thus not included in the CI basis. Figure 4 shows some important matrix elements, including J_{gg} (Coulomb energy of σ_g MO), J_{gu} (Coulomb energy between σ_g and σ_u), and K_{gu} (exchange energy between σ_g and σ_u). The Coulomb energy between σ_u MO, J_{uu} is nearly identical to J_{gg} and therefore is not plotted. Diagonalizing the all-bound-state CI

problem gives the two-particle states, shown in Fig.5a. We give all six Σ states (where both electrons occupy the σ states) and the two lowest three-fold degenerate $^3\Pi_u$ states (where one electron occupies the σ_g and one occupies one of the π levels). We observe that:

(a) The ground-state is singlet $^1\Sigma_g^{(a)}$ for all dot-dot distances. However, the character of the state is very different at different inter-dot separation d , which can be analyzed by the isospin of the state,³² defined as the difference in the number of electrons occupying the bonding (N_B) and antibonding (N_{AB}) states in a given CI state, i.e. $I_z = (N_B - N_{AB})/2$, where N_B and N_{AB} are obtained from Eq.(5). As shown in Fig.6, $I_z(d)$ of the $^1\Sigma_g^{(a)}$ state is very different at different inter-dot distances: At small inter-dot distance, the dominant configuration of the ground state is $|\sigma_g^\uparrow, \sigma_g^\downarrow\rangle$ (both electrons occupy bonding state and $N_B=2$), and $I_z \sim 1$. However, in the weak coupling region, there is significant mixing of bonding σ_g and anti-bonding states σ_u , and I_z is smaller than 1, e.g. $I_z \sim 0.2$ at $d = 9.5$ nm. At infinite separation, where the bonding and antibonding states are degenerate, one expects $I_z \rightarrow 0$.

(b) Next to the ground state, we find in Fig.5a the three-fold degenerate triplet states $^3\Sigma_u$, with $S_z = 1, -1$ and 0 . In the absence of spin-orbit coupling, triplet states will not couple to singlet states. If we include spin-orbit coupling, the triplet may mix with the singlet state, and the degeneracy will be lifted. At large inter-dot distances, the ground state singlet $^1\Sigma_g^{(a)}$ and triplet states $^3\Sigma_u$ are degenerate. The splitting of total CI energy between ground state singlet and triplet $J_{S-T} = E(^3\Sigma) - E(^1\Sigma_g)$ is plotted in Fig.3 on a logarithmic scale. As we can see, J_{S-T} also decays approximately exponentially between 4 and 8 nm, and can be fitted as $J_{S-T} = 5.28 \exp(-d/0.965)$ eV. The decay length of 0.965 nm is shorter than the decay length 1.15 nm of Δ_σ . At small inter-dot separations, $J_{S-T} \sim \Delta_\sigma$ in Fig.3, as expected from a simple Heitler-London model.⁹

(c) The two excited singlet states originating from the occupation of σ_u anti-bonding states, $^1\Sigma_u$ and $^1\Sigma_g^{(b)}$ are further above the $^3\Sigma_u$ state.

(d) The lowest $^3\Pi_u$ states are all triplet states. They

are energetically very close to each other since we have two nearly degenerate π_u MO states. In the weak coupling region, the Π_u states are well above the Σ states, as a consequence of large single-particle energy difference $\epsilon(\pi_u) - \epsilon(\sigma_u)$. However, the Π_u , and $^1\Sigma_g^{(b)}$ cross at about 4.5 nm, where the single-particle MO level π_u is still much higher than σ_u . In this case, the Coulomb correlations have to be taken into account.

In the following sections, we enquire as to possible simplifications over the all-bound-states CI treatment.

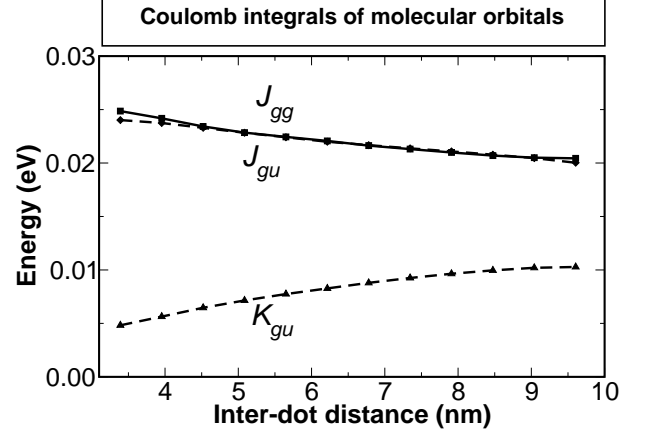


FIG. 4: Selected Coulomb integrals for molecular orbitals. J_{gg} is the self-Coulomb energy of the σ_g orbital and J_{gu} is the Coulomb energy between σ_g and σ_u orbitals, while K_{gu} is the exchange energy between σ_g and σ_u orbitals.

B. Level-2 theory: reduced CI in the molecular basis

In Level-2 theory, we will reduce the full 66×66 CI problem of Level-1 to one that includes only the σ_g and σ_u basis, giving a 6×6 CI problem. The six many-body basis states are shown in Fig.1a, $|a\rangle = |\sigma_g^\uparrow, \sigma_u^\uparrow\rangle$, $|b\rangle = |\sigma_g^\downarrow, \sigma_u^\downarrow\rangle$, $|c\rangle = |\sigma_g^\uparrow, \sigma_u^\downarrow\rangle$, $|d\rangle = |\sigma_g^\downarrow, \sigma_u^\uparrow\rangle$, $|e\rangle = |\sigma_g^\uparrow, \sigma_g^\downarrow\rangle$, $|f\rangle = |\sigma_u^\uparrow, \sigma_u^\downarrow\rangle$. In this basis set, the CI problem is reduced to a 6×6 matrix eigenvalue equation,

$$H = \begin{pmatrix} \epsilon_g + \epsilon_u + J_{gu} - K_{gu} & 0 & 0 & 0 & 0 & 0 \\ 0 & \epsilon_g + \epsilon_u + J_{gu} - K_{gu} & 0 & 0 & 0 & 0 \\ 0 & 0 & \epsilon_g + \epsilon_u + J_{gu} & -K_{gu} & -\Gamma_{gg}^{gu} & -\Gamma_{uu}^{gu} \\ 0 & 0 & -K_{gu} & \epsilon_g + \epsilon_u + J_{gu} & \Gamma_{gg}^{gu} & \Gamma_{uu}^{gu} \\ 0 & 0 & -\Gamma_{gg}^{gu} & \Gamma_{gg}^{gu} & 2\epsilon_g + J_{gg} & \Gamma_{uu}^{gg} \\ 0 & 0 & -\Gamma_{uu}^{gu} & \Gamma_{uu}^{gu} & \Gamma_{gg}^{uu} & 2\epsilon_u + J_{uu} \end{pmatrix} \quad (13)$$

where, ϵ_g and ϵ_u are the single-particle energy levels for the MO's $|\sigma_g\rangle$ and $|\sigma_u\rangle$, respectively. In the absence of

spin-orbit coupling, the triplet states $|a\rangle$ and $|b\rangle$ are not coupled to any other states, as required by the total spin

conservation, and thus they are already eigenstates. The rest of the matrix can be solved using the integrals calculated from Eq.(4). The results of the 6×6 problem were compared to the all-bound-state CI results: We find that the Σ states of Level-2 theory are very close to those of the all-bound-state CI calculations, indicating a small coupling between σ and π orbitals in the *strong confinement* region. We thus do not show graphically the results of Level-2. However, since we use only σ orbitals, the Π states of Level-1 (Fig.5a) are absent in Level-2 theory. Especially, the important feature of crossover between Σ and Π_u states at 4 and 4.5 nm is missing.

C. Level-3 theory: single-configuration in the molecular basis

As is well known, mean-field-like treatments such as RHF and LSD usually give incorrect dissociation behavior of molecules, as the correlation effects are not adequately treated. Given that RHF and LSD are widely used in studying QMDs,^{10,13,14} it is important to understand under which circumstance the methods will succeed and under which circumstance they will fail in describing the few-electron states in a QDM. In level-3 theory, we thus mimic the mean-field theory by further ignoring the *off-diagonal* Coulomb integrals in Eq.(13) of Level-2 theory, i.e., we assume $\Gamma_{uu}^{gu} = \Gamma_{gg}^{gu} = \Gamma_{gg}^{uu} = 0$. This approximation is equivalent to ignoring the coupling between different configurations, and is thus called “single-configuration” (SC) approximation. At the SC level, we have very simple analytical solutions of the two-electron states,

$$E(1\Sigma_g^{(a)}) = 2\epsilon_g + J_{gg}; \quad |1\Sigma_g^{(a)}\rangle = |e\rangle, \quad (14)$$

$$E(3\Sigma_u) = (\epsilon_g + \epsilon_u) + J_{gu} - K_{gu}; \quad \begin{cases} |3\Sigma_u^+\rangle = |a\rangle, \\ |3\Sigma_u^-\rangle = |b\rangle, \\ |3\Sigma_u^0\rangle = |c\rangle - |d\rangle, \end{cases} \quad (15)$$

$$E(1\Sigma_u) = (\epsilon_g + \epsilon_u) + J_{gu} + K_{gu}; \quad |1\Sigma_u\rangle = |c\rangle + |d\rangle \quad (16)$$

$$E(1\Sigma_g^{(b)}) = 2\epsilon_u + J_{uu}; \quad |1\Sigma_g^{(b)}\rangle = |f\rangle. \quad (17)$$

The energies are plotted in Fig.5b. When comparing the Σ states of the SC approach to the all-bound-state CI results in Fig.5a, we find good agreement in the strong coupling region for $d \leq 5$ nm (see Fig.3). However, the SC approximation fails qualitatively at larger inter-dot separations in two aspects: (i) The order of singlet state $1\Sigma_g^{(a)}$ and triplet state $3\Sigma_u$ is reversed (see Fig. 5b,c). (ii) The $1\Sigma_g^{(a)}$ and $3\Sigma_u$ states fail to be degenerate at large interdot separation. This lack of degeneracy is also observed for $1\Sigma_g^{(b)}$ and $1\Sigma_u$. These failures are due to the absence of correlations in the SC approximation. Indeed as shown in Fig.6, the accurate Level-1 ground state singlet has considerable mixing of anti-bonding states, i.e. $I_z \rightarrow 0$ at large d . However, in the SC approximation both electrons are *forced* to occupy the σ_g orbital in the lowest singlet state $1\Sigma_g^{(a)}$ as a consequence of the lack of

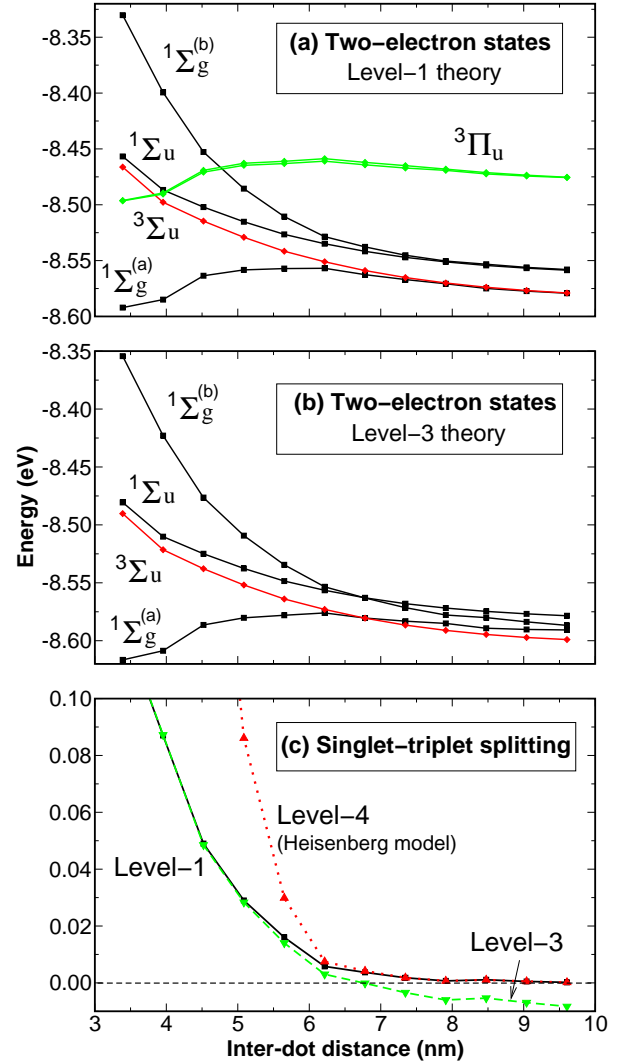


FIG. 5: (Color online) (a) Two-electron states calculated from CI using all confined MO from LCBB (Level-1), including the singlet $1\Sigma_g^{(a)}$, $1\Sigma_u$, $1\Sigma_g^{(b)}$ states and the 3-fold degenerated triplet states $3\Sigma_u$ as well as two 3-fold degenerated triplet states $3\Pi_u$. (b) Two electron states calculated from the single-configuration approximation (Level-3). (c) Comparison of the singlet-triplet splitting calculated from Levels 1, 3 and 4 theories.

the coupling between the configuration $|e\rangle$ of Fig.1a and other configurations. As a result, in Level-3 theory, the isospins are forced to be $I_z=1$ for $1\Sigma_g^{(a)}$ at all inter-dot distances d , which pushes the singlet energy higher than the triplet.

D. Level-4 theory: Hubbard model and Heisenberg model in a dot-centered basis

The Hubbard model and the Heisenberg model are often used⁵ to analyze entanglement and gate operations

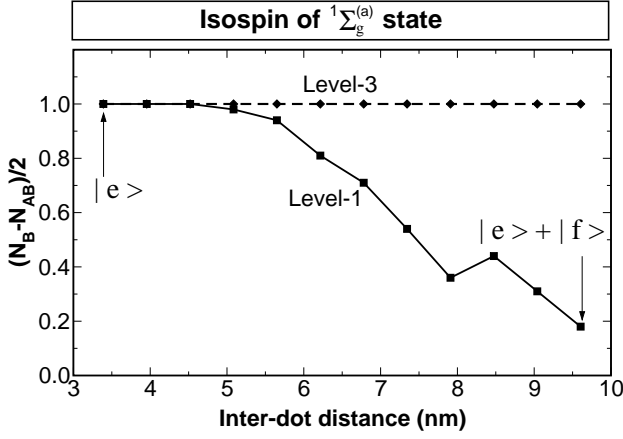


FIG. 6: Isospin, defined as the difference in the number of electrons occupying the bonding (N_B) and antibonding (N_{AB}) states, of the $1\Sigma_g^{(a)}$ state in Level-1 and Level-3 theories.

for two spins qubits in a QDM. Here, we analyze the extent to which such approaches can correctly capture the qualitative physics given by more sophisticated models. Furthermore, by doing so, we obtain the parameters of the models from realistic calculations.

1. Transforming the states to a dot-centered basis

Unlike the Level 1 - 3 theories, the Hubbard and the Heisenberg models are written in a dot-centered basis as shown in Fig.1b, rather than in the molecular basis of Fig.1a. In a dot-centered basis, the Hamiltonian of Eq.(3) can be rewritten as,

$$H = \sum_{\eta_1, \eta_2} \sum_{\sigma} (e_{\eta_1} \delta_{\eta_1 \eta_2} + t_{\eta_1 \eta_2}) \chi_{\eta_1, \sigma}^{\dagger} \chi_{\eta_2, \sigma} + \frac{1}{2} \sum_{\eta_1, \dots, \eta_4} \sum_{\sigma, \sigma'} \tilde{\Gamma}_{\eta_3, \eta_4}^{\eta_1, \eta_2} \chi_{\eta_1, \sigma}^{\dagger} \chi_{\eta_2, \sigma'}^{\dagger} \chi_{\eta_3, \sigma'} \chi_{\eta_4, \sigma}, \quad (18)$$

where, $\eta = (l, p)$ and $\chi_{\eta, \sigma}^{\dagger}$ creates an electron in the $l=(s, p, \dots)$ orbital on the $p=(T, B)$ dot with spin σ that has single-particle energy e_{η} . Here, $t_{\eta_1 \eta_2}$ is the coupling between the η_1 and η_2 orbitals, and $\tilde{\Gamma}_{\eta_3, \eta_4}^{\eta_1, \eta_2}$ is the Coulomb integral of single-dot orbitals χ_{η_1} , χ_{η_2} , χ_{η_3} and χ_{η_4} .

We wish to construct a Hubbard Hamiltonian whose parameters are taken from the fully atomistic single-particle theory. To obtain such parameters in Eq.(18) including e_{η} , $t_{\eta_1 \eta_2}$ and $\tilde{\Gamma}_{\eta_3, \eta_4}^{\eta_1, \eta_2}$, we resort to a Wannier-like transformation, which transform the “molecular” orbitals (Fig.1a) into single-dot “atomic” orbitals (Fig.1b). The latter dot-centered orbitals are obtained from a unitary rotation of the *molecular* orbitals ψ_i , i.e.,

$$\chi_{\eta} = \sum_{i=1} \mathcal{U}_{\eta, i} \psi_i, \quad (19)$$

where, ψ_i is the i -th molecular orbitals, χ_{η} is the single dot-centered orbitals, and \mathcal{U} are unitary matrices, i.e. $\mathcal{U}^{\dagger} \mathcal{U} = I$. We chose the unitary matrices that maximize the total orbital self-Coulomb energy. The procedure of finding these unitary matrices is described in detail in Appendix A. The dot-centered orbitals constructed this way are approximately invariant to the change of coupling between the dots.³³ Once we have the \mathcal{U} matrices, we can obtain all the parameters in Eq.(18) by transforming them from the molecular basis. The Coulomb integrals in the new basis set are given by Eq. (A2), while other quantities including the effective single-particle levels e_{η} for the η -th dot-centered orbital, and the coupling

between the η_1 -th and η_2 -th orbitals $t_{\eta_1 \eta_2}$ can be obtained from,

$$e_{\eta} = \langle \chi_{\eta} | \hat{T} | \chi_{\eta} \rangle = \sum_i \mathcal{U}_{\eta, i}^* \mathcal{U}_{\eta, i} \epsilon_i, \quad (20)$$

$$t_{\eta_1 \eta_2} = \langle \chi_{\eta_1} | \hat{T} | \chi_{\eta_2} \rangle = \sum_i \mathcal{U}_{\eta_1, i}^* \mathcal{U}_{\eta_2, i} \epsilon_i, \quad (21)$$

where ϵ_i is the single-particle level of the i -th *molecular* orbital, and \hat{T} is kinetic energy operator. Using the transformation of Eq.(20), Eq.(21) and Eq.(A2), we calculate all parameters of Eq.(18). Figure 7a, shows the effective single-dot energy of the “s” orbitals obtained in the Wannier representation for both top and bottom dots. We see that the effective single-dot energy levels increase rapidly for small d . Furthermore the energy levels for the top and bottom orbitals are split due to the strain asymmetry between the two dots. We compute the Coulomb energies J_{TT} , J_{BB} of the “s” orbitals on both top and bottom dots, and the inter-dot Coulomb and exchange energies J_{TB} and K_{TB} and plot these quantities in Fig. 7b. Since J_{TT} and J_{BB} are very similar, we plot only J_{TT} . As we can see, the Coulomb energies of the dot-centered orbitals are very close to the Coulomb energy of the s orbitals of a *isolated* single dot (dashed line). The inter-dot Coulomb energy J_{TB} has comparable amplitude to J_{TT} and decays slowly with distance, and remain very significant, even at large separations. However, the exchange energy between the orbitals localized on top dot and bottom dot K_{TB} is extremely small even when the dots are very close.

2. “First-principles” Hubbard model and Heisenberg model: Level-4

In level-4 approximation, we use only the “s” orbital in each dot. Figure 1b shows all possible many-body basis

$$H = \begin{pmatrix} e_T + e_B + J_{TB} - K_{TB} & 0 & 0 & 0 & 0 & 0 \\ 0 & e_T + e_B + J_{TB} - K_{TB} & 0 & 0 & 0 & 0 \\ 0 & 0 & e_T + e_B + J_{TB} & -K_{TB} & t - \tilde{\Gamma}_{BB}^{TB} & t - \tilde{\Gamma}_{TT}^{TB} \\ 0 & 0 & -K_{TB} & e_T + e_B + J_{TB} & -t + \tilde{\Gamma}_{BB}^{TB} & -t + \tilde{\Gamma}_{TT}^{TB} \\ 0 & 0 & t - \tilde{\Gamma}_{TB}^{BB} & -t + \tilde{\Gamma}_{TB}^{BB} & 2e_B + J_{BB} & 0 \\ 0 & 0 & t - \tilde{\Gamma}_{TB}^{TT} & -t + \tilde{\Gamma}_{TB}^{TT} & 0 & 2e_T + J_{TT} \end{pmatrix}. \quad (22)$$

where $t = t_{TB}$ and to simplify the notation, we ignore the orbital index “s”. If we keep all the matrix elements, the description using the molecular basis of Fig. 1a and the dot localized basis of Fig. 1b are equivalent, since they are connected by unitary transformations. We now simplify Eq.(22) by ignoring the off-diagonal Coulomb integrals. The resulting Hamiltonian is the single-band Hubbard model. Unlike Level-3 theory, in this case, ignoring off-diagonal Coulomb integrals (but keeping hopping) can still give qualitatively correct results, due to the fact that off-diagonal Coulomb integrals such as $\tilde{\Gamma}_{TB}^{BB} \ll t$, and the correlation is mainly carried by inter-dot hopping t . We can further simplify the model by assuming $e_T = e_B = \epsilon$; $J_{TT} = J_{BB} = U$; and let $J_{TB} = V$, $K_{TB} = K$. We can then solve the simplified eigenvalue equation analytically. The eigenvalues of the above Hamiltonian are (in order of increasing energy):

1. Ground state singlet $^1\Sigma_g^{(a)}$

$$E = 2\epsilon + \frac{1}{2}[U + V + K - \sqrt{16t^2 + (U - V - K)^2}] \quad (23)$$

2. Triplet states (three-fold degenerate) $^3\Sigma_u$

$$E = 2\epsilon + V - K \quad (24)$$

3. Singlet $^1\Sigma_u$

$$E = 2\epsilon + U \quad (25)$$

4. Singlet $^1\Sigma_g^{(b)}$

$$E = 2\epsilon + \frac{1}{2}[U + V + K + \sqrt{16t^2 + (U - V - K)^2}] \quad (26)$$

In the Hubbard limit where Coulomb energy $U \gg t$, the singlet-triplet splitting $J_{S-T} = E(^3\Sigma) - E(^1\Sigma_g) \sim 4t^2/(U - V)$, which reduces the model to the Heisenberg model

$$H = \frac{4t^2}{U - V} \vec{S}_T \cdot \vec{S}_B, \quad (27)$$

functions of two electrons, where top and bottom dots are denoted by “T” and “B” respectively. The Hamiltonian in this basis set is,

where \vec{S}_T and \vec{S}_B are the spin vectors on the top and bottom dots. The Heisenberg model gives the correct order for singlet and triplet states. The singlet-triplet splitting $J_{S-T} = 4t^2/(U - V)$ is plotted in Fig. 5c and compared to the results from all-bound-state CI calculations (Level-1), and single-configuration approximations (Level-3). As we can see, at $d > 6.5$ nm, the agreement between the Heisenberg model with CI is good, but the Heisenberg model greatly overestimates J_{S-T} at $d < 6$ nm.

E. Comparison of pair correlation functions for Levels 1-4 theories

In the previous sections, we compared the energy levels of two-electron states in several levels of approximations to all-bound-state CI results (Level-1). We now provide further comparison of Levels 1-4 theories by analyzing the pair correlation functions and calculating the electron-electron entanglement at different levels of approximations.

In Fig. 8 we show the pair correlation functions of Eq.(6) for the $^1\Sigma_g^{(a)}$ and $^1\Sigma_g^{(b)}$ states at $d \sim 7$ nm for Level-1 and Level-3 theories. The correlation functions give the probability of finding the second electron when the first electron is fixed at the position shown by the arrows at the center of the bottom dot (left hand side of Fig. 8) or the top dot (right hand side of Fig. 8). Level-1 and Level-2 theories give correlation-induced electron localization at large d : for the $^1\Sigma_g^{(a)}$ state, the two electrons are localized on different dots, while for the $^1\Sigma_g^{(b)}$ state, both electrons are localized on the same dot.²⁰ In contrast, Level-3 theory shows delocalized states because of the lack of configuration mixing. This problem is shared by RHF and LSD approximations.

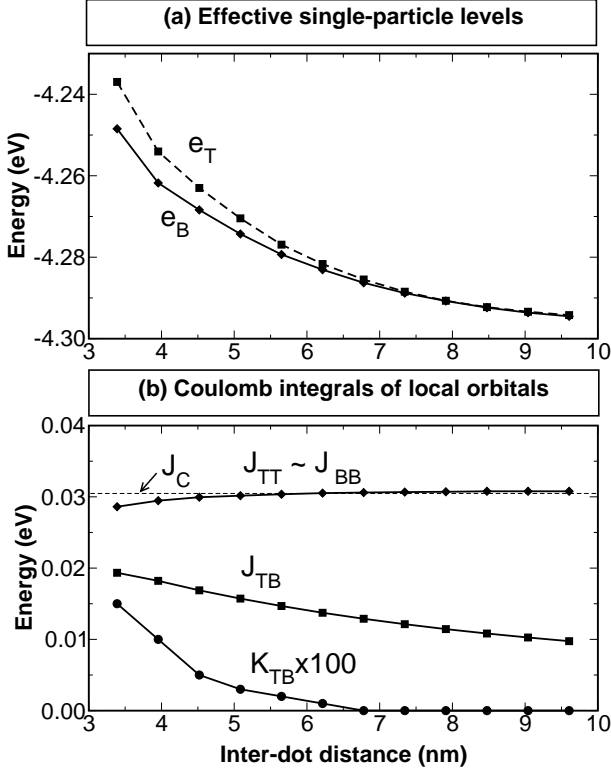


FIG. 7: (a) Effective single-particle energy levels of s orbitals localized on the top (e_T) and bottom (e_B) dots. (b) Intra-dot Coulomb energy J_{TT} , J_{BB} , inter-dot Coulomb energy J_{TB} and inter-dot exchange energy K_{TB} (magnified by a factor 100). The dashed line gives the single orbital self-Coulomb energy J_C .

F. Comparison of the degree of entanglement for Levels 1-4 theories

The DOE of the four “ Σ ” states are plotted in Fig.9 for Level-1, Level-3 and Level-4 theories; the DOE of Level-2 theory are virtually identical to those of Level-1 theory, and are therefore not plotted. We see that the Hubbard model has generally reasonable agreement with Level-1 theory while the DOE calculated from Level-3 and Level-4 (Heisenberg model) theories deviate significantly from the Level-1 theory, which is addressed below:

(i) *The $^1\Sigma_g^{(a)}$ state:* The Level-1 theory (Fig.9a), shows that the DOE of $^1\Sigma_g^{(a)}$ increases with d and approaches 1 at large d . The Hubbard model of Level-4 theory (Fig.9c) gives qualitatively correct DOE for this state except for some details. However, Level-3 theory (Fig.9b) gives DOE $\mathcal{S} = 0$ because the wavefunction of $^1\Sigma_g^{(a)}$ is a single Slater determinant $|e\rangle$ [see Eq.(14)]. For the same reason, the DOEs of the $^1\Sigma_g^{(a)}$ state in RHF and LSD approximations are also zero as a consequence of lack of correlation. In contrast, the Heisenberg model of Level-4 theory gives $\mathcal{S}(^1\Sigma_g^{(a)}) = 1$. This is because the Heisenberg model assumes that the both electrons are localized

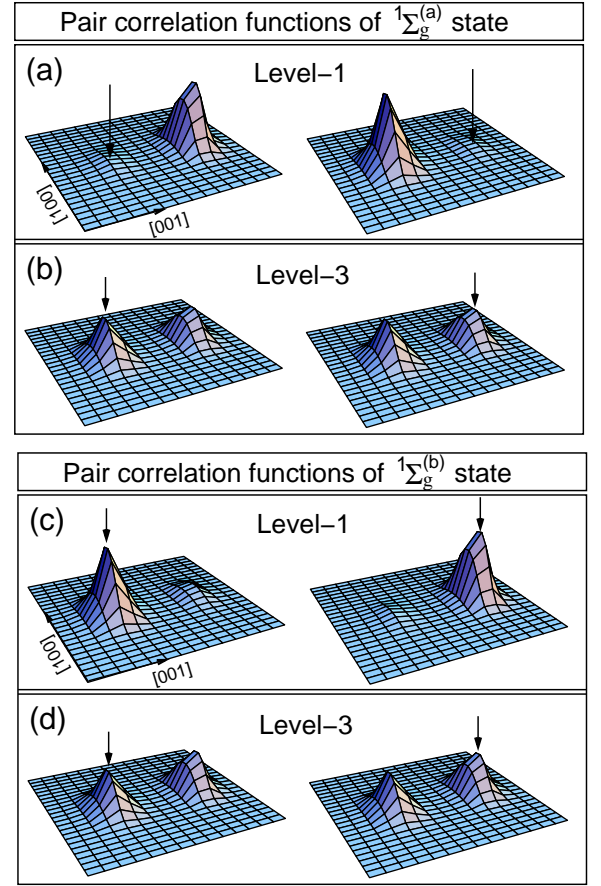


FIG. 8: (Color online) Comparison of pair correlation functions calculated from (a) Level-1, (b) Level-3 theory for the $^1\Sigma_g^{(a)}$ state and (c) Level-1, (d) Level-3 theory for the $^1\Sigma_g^{(b)}$ state at $d \sim 7$ nm. On the left hand side, the first electron is fixed at the center of the bottom dot, while on the right hand side, the first electron is fixed at the center of the top dot, as indicated by the arrows.

on different dots with zero double occupancy, and thus overestimates the DOE.^{20,34}

(ii) *The $^1\Sigma_g^{(b)}$ state:* The Hubbard model gives the DOE of the $^1\Sigma_g^{(b)}$ state identical to that of $^1\Sigma_g^{(a)}$ state. This is different from the result of Level-1 theory, especially at large inter-dot separations. The difference comes from the assumption in the Hubbard model that the energy levels and wavefunctions on the top dot and on the bottom dot are identical while as discussed in Ref.20, the wavefunctions are actually asymmetric due to inhomogeneous strain in the real system. At $d > 8$ nm, the $^1\Sigma_g^{(b)}$ state is the supposition of $|E\rangle$ and $|F\rangle$ configurations in the Hubbard model leading to $\mathcal{S} = 1$, while in Level-1 theory, the two electrons are both localized on the *top* dots ($|F\rangle$) at $d > 9$ nm,²⁰ resulting in near zero entanglement. For the same reason discussed in (i), the Level-3 theory gives $\mathcal{S}(^1\Sigma_g^{(b)}) = 0$.

(iii) *The $^1\Sigma_u$ state:* Both the Level-3 theory and Hubbard model give $\mathcal{S}(^1\Sigma_u) = 1$. However, the $\mathcal{S}(^1\Sigma_u)$ of

the Level-1 theory has more features as the consequence of the asymmetry of the system. In contrast to the $1\Sigma_g^{(b)}$ state, in the $1\Sigma_u$ state, both electrons are localized on the *bottom* dot leading to near zero entanglement at $d > 9$ nm.

(iv) *The $3\Sigma_u$ state:* All levels of theories give very close results of DOE for $3\Sigma_u$ state. Actually, in Level-1 theory, the DOE of $3\Sigma_u$ state is only slightly larger than 1, indicating weak entanglement of the σ and π orbitals (the maximum entanglement one can get from the total of six orbitals is $\mathcal{S}_{\max} = \log_2 6$), while in all other theories (including the Level-2 theory) they are exactly 1 since these theories include only two σ orbitals. The small coupling between σ and π orbitals is desirable for quantum computation, which requires the qbits states to be decoupled from other states.

IV. SUMMARY

We have shown the energy spectrum, pair-correlation functions and degree of entanglement of two-electron states in self-assembled InAs/GaAs quantum dot molecules *via* all-bound-state configuration interaction calculations and compared these quantities in different levels of approximations. We find that the correlation between electrons in the top and bottom dot is crucial to get the qualitative correct results for both the singlet-triplet splitting and the degree of entanglement. The single-configuration approximation and similar theories such as RHF, LSD all suffer from lack of correlation and thus give incorrect ground state, singlet-triplet splitting J_{S-T} and degree of entanglement. Highly simplified models, such as the Hubbard model gives qualitatively correct results for the ground state and J_{S-T} , while the Heisenberg model only give similar results at large d . These two models are written in the dot-centered basis, where the correlation between the top and bottom dots are carried by the single-particle tunneling. However, as a consequence of ignoring the asymmetry present in the real system, the degree of entanglement calculated from the Hubbard model deviates significantly from realistic atomic calculations. Moreover the Heisenberg model greatly overestimates the degree of entanglement of the ground state as a consequence of further ignoring the electron double occupancy in the dot molecule.

Acknowledgments

This work was supported by US DOE-SC-BES-DMS, under LAB 3-17 initiative Grant No. DEAC36-98-GO10337.

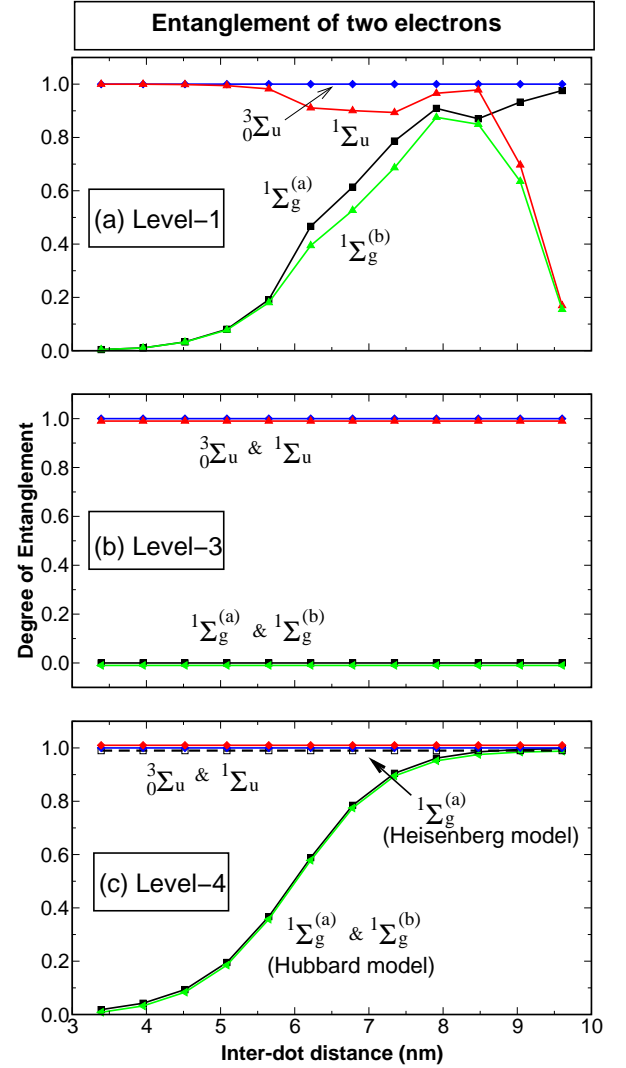


FIG. 9: (Color online) Comparison of the DOE calculated from (a) Level-1; (b) Level-3 and (c) Level-4 theories for two-electron states. In panel (c), both the DOE of the Hubbard model (solid lines) and of the Heisenberg model for $1\Sigma_g^{(a)}$ state (dashed line) are shown.

APPENDIX A: CONSTRUCTION OF DOT-CENTERED ORBITALS

When we solve the single-particle Eq.(1) for the QDM, we get a set of molecular orbitals. However sometimes we need to discuss the physics in a dot-localized basis set. The dot-localized orbitals χ_η can be obtained from a unitary rotation of molecular orbitals,

$$\chi_\eta = \sum_{i=1}^N \mathcal{U}_{\eta,i} \psi_i, \quad (\text{A1})$$

where, ψ_i is the i -th molecular orbital, and \mathcal{U} is a unitary matrix, i.e. $\mathcal{U}^\dagger \mathcal{U} = I$. To obtain a set of well localized orbitals, we require that the unitary matrix \mathcal{U} maximizes

the total orbital self-Coulomb energy. The orbitals fulfilling the requirement are approximately invariant under the changes due to coupling between the dots.³³ For a given unitary matrix \mathcal{U} , the Coulomb integrals in the rotated basis are,

$$\tilde{\Gamma}_{\eta_3, \eta_4}^{\eta_1, \eta_2} = \sum_{i,j,k,l} \mathcal{U}_{\eta_1, i}^* \mathcal{U}_{\eta_2, j}^* \mathcal{U}_{\eta_3, k} \mathcal{U}_{\eta_4, l} \Gamma_{k,l}^{i,j}, \quad (\text{A2})$$

where $\Gamma_{k,l}^{i,j}$ are the Coulomb integrals in the molecular basis. Thus, the total self-Coulomb energy for the orbitals $\{\chi_\eta\}$ is:

$$U_{\text{tot}} = \sum_{\eta} \tilde{\Gamma}_{\eta, \eta}^{\eta, \eta} = \sum_{\eta} \sum_{i,j,k,l} \mathcal{U}_{\eta, i}^* \mathcal{U}_{\eta, j}^* \mathcal{U}_{\eta, k} \mathcal{U}_{\eta, l} \Gamma_{k,l}^{i,j}. \quad (\text{A3})$$

The procedure of finding the unitary matrix \mathcal{U} that maximizes U_{tot} is similar to the procedure given in Ref. 35

where the maximally localized Wannier functions for extended systems are constructed using a different criteria. Starting from $\mathcal{U} = I$, we find a new $\mathcal{U} = I + \delta\epsilon$ that increases U_{tot} . To keep the new matrix unitary, we require $\delta\epsilon$ to be a small anti-Hermitian matrix. It is easy to prove that

$$G_{i,j} \equiv \frac{\delta U_{\text{tot}}}{\delta \epsilon_{j,i}} = \Gamma_{i,j}^{j,j} + \Gamma_{j,i}^{j,j} - \Gamma_{i,i}^{i,j} - \Gamma_{i,i}^{j,i} \quad (\text{A4})$$

and to verify that $G_{i,j} = -G_{j,i}^*$. By choosing $\delta\epsilon_{i,j} = -\epsilon G_{i,j}$, where ϵ is a small real number, we always have (to the first-order of approximation) $\Delta U_{\text{tot}} = \epsilon \|G\| \geq 0$, i.e. the procedure always increases the total self-Coulomb energy. To keep the strict unitary character of the \mathcal{U} matrices in the procedure, the \mathcal{U} matrices are actually updated as $\mathcal{U} \leftarrow \mathcal{U} \exp(-\epsilon G)$, until the localization is achieved.

-
- ¹ M. Pi, A. Emperador, M. Barranco, F. Garcias, K. Muraki, S. Tarucha, and D. G. Austing, Phys. Rev. Lett. **87**, 066801 (2001).
 - ² M. Rontani, S. Amaha, K. Muraki, F. Manghi, E. Molinari, S. Tarucha, and D. G. Austing, Phys. Rev. B **69**, 085327 (2004).
 - ³ F. R. Waugh, M. J. Berry, D. J. Mar, M. Westervelt, K. L. Campman, and A. C. Gossard, Phys. Rev. Lett. **75**, 705 (1995).
 - ⁴ M. Bayer, P. Hawrylak, K. Hinzer, S. Fafard, M. Korkusinski, Z. R. Wasilewski, O. Stern, and A. Forchell, Science **291**, 451 (2001).
 - ⁵ D. Loss and D. P. DiVincenzo, Phys. Rev. A **57**, 120 (1998).
 - ⁶ R. C. Ashoori, H. L. Stormer, J. S. Weiner, L. N. Pfeiffer, S. J. Pearton, K. W. Baldwin, and K. W. West, Phys. Rev. Lett. **68**, 3088 (1992).
 - ⁷ A. T. Johnson, L. P. Kouwenhoven, W. de Jong, N. van der Vaart, and C. J. P. M. Harmans, Phys. Rev. Lett. **69**, 1592 (1992).
 - ⁸ S. Tarucha, D. G. Austing, T. Honda, R. J. van der Hage, and L. P. Kouwenhoven, Phys. Rev. Lett. **77**, 3613 (1996).
 - ⁹ G. Burkard and D. Loss, Phys. Rev. B **59**, 2070 (1999).
 - ¹⁰ H. Tamura, Physica B **249-251**, 210 (1998).
 - ¹¹ C. Yannouleas and U. Landman, Phys. Rev. Lett. **82**, 5325 (1999).
 - ¹² X. Hu and S. D. Sarma, Phys. Rev. A **61**, 62301 (2000).
 - ¹³ S. Nagaraja, J. P. Leburton, and R. M. Martin, Phys. Rev. B **60**, 8759 (1999).
 - ¹⁴ B. Partoens and F. M. Peeters, Phys. Rev. Lett. **84**, 4433 (2000).
 - ¹⁵ M. Rontani, F. Troiani, U. Hohenester, and E. Molinari, Solid State Comm. **119**, 309 (2001).
 - ¹⁶ T. Ota, M. Stopa, M. Rontani, T. Hatano, K. Yamada, S. Tarucha, H. Song, Y. Nakata, T. Miyazawa, T. Ohshima, et al., Superlattices and Microstructures **34**, 159 (2003).
 - ¹⁷ T. Ota, K. Ono, M. Stopa, T. Hatano, S. Tarucha, H. Z. Song, Y. Nakata, T. Miyazawa, T. Ohshima, and N. Yokoyama, Phys. Rev. Lett. **93**, 66801 (2004).
 - ¹⁸ L. W. Wang, A. J. Williamson, A. Zunger, H. Jiang, and J. Singh, Appl. Phys. Lett. **76**, 339 (2000).
 - ¹⁹ G. Bester, J. Shumway, and A. Zunger, Phys. Rev. Lett. **93**, 047401 (2004).
 - ²⁰ L. He, G. Bester, and A. Zunger, to be published (cond-mat/0412172).
 - ²¹ P. N. Keating, Phys. Rev. **145**, 637 (1966).
 - ²² J. L. Martins and A. Zunger, Phys. Rev. B **30**, 6217 (1984).
 - ²³ A. J. Williamson, L.-W. Wang, and A. Zunger, Phys. Rev. B **62**, 12963 (2000).
 - ²⁴ L. He, G. Bester, and A. Zunger, Phys. Rev. B **70**, 235316 (2004).
 - ²⁵ L.-W. Wang and A. Zunger, Phys. Rev. B **59**, 15806 (1999).
 - ²⁶ A. Franceschetti, H. Fu, L.-W. Wang, and A. Zunger, Phys. Rev. B **60**, 1819 (1999).
 - ²⁷ M. A. Nielsen and I. L. Chuang, *Quantum Computation and Quantum Information* (Cambridge University Press, Cambridge, 2000).
 - ²⁸ C. Bennett, H. Bernstein, S. Popescu, and B. Shumacher, Phys. Rev. A **53**, 2046 (1996).
 - ²⁹ L. H. et al, to be published.
 - ³⁰ C. N. Yang, Rev. Mod. Phys. **34**, 694 (1962).
 - ³¹ J. Schliemann, J. I. Cirac, M. Kuś, M. Lewenstein, and D. Loss, Phys. Rev. A **64**, 022303 (2001).
 - ³² J. J. Palacios and P. Hawrylak, Phys. Rev. B **51**, 1769 (1995).
 - ³³ C. Edmiston and K. Ruedenberg, Rev. Mod. Phys. **35**, 457 (1963).
 - ³⁴ J. Schliemann, D. Loss, and A. H. MacDonald, Phys. Rev. B **63**, 085311 (2001).
 - ³⁵ N. Marzari and D. Vanderbilt, Phys. Rev. B **56**, 12847 (1997).